Oxyanion Behavior in Alkaline Environments: Sorption and Desorption of Arsenate in Ettringite

SATISH C. B. MYNENI,*,† SAMUEL J. TRAINA,† TERRY J. LOGAN,† AND GLENN A. WAYCHUNAS‡

Environmental Sciences, School of Natural Resources, 202 Kottman Hall, 2021 Coffey Road, The Ohio State University, Columbus, Ohio 43210, and Center for Materials Research, McCullogh Building, Stanford University, Stanford, California 94305

Arsenate sorption by ettringite [$Ca_6Al_2(SO_4)_3(OH)_{12}\cdot 26H_2O$] is examined as adsorption and coprecipitation systems at alkaline pH (10.0−12.5) and for a wide range of As(V) concentration (<1 μM−15 mM). The mode of sorption and sorbate and sorbent concentrations controlled the nature of solid-phase As(V) speciation. Although high pH increased ettringite stability in concentrated As(V) solutions, it did not influence total As(V) sorption. During adsorption, ettringite exposure to concentrated As(V) solutions (>2.0 mM) precipitated new unidentified microcrystalline minerals at the expense of ettringite. Concentrated As(V) solution exposure to coprecipitating ettringite poisoned ettringite crystal growth, with precipitation of some microcrystalline minerals. Sorbed As(V) was also not desorbable in the presence of concentrated sulfate and high ionic strength solutions. Details of As(V) adsorption and coprecipitation systems and inferences on As(V) molecular interactions are proposed.

Introduction

Arsenate [As(V)] is a common soil contaminant and has high mobility in alkaline environments. This behavior is due to its repulsion by negatively charged soil and sediment particle surfaces (*1*−*3*). At near-neutral pH, minerals such as goethite, ferrihydrite, schwertmannite, and other iron oxides (*4*−*8*) sorb significant quantities of As(V). On the contrary, few mineral surfaces have been reported to sorb As(V) in alkaline environments. Studies on weathered fly ashes, cements, and alkaline soils have identified calcite ($CaCO_3$), portlandite [$Ca(OH)_2$], and ettringite [$Ca_6Al_2(SO_4)_3(OH)_{12}\cdot 26H_2O$] as stable mineral phases controlling trace element solubility in these high pH regimes (*9*−*15*). Carbonation and induced calcite precipitation from dolomite decreased As(V) concentration in As(V)-contaminated waste waters (*13*), but the responsible reaction mechanisms have not been ascertained (*9*, *14*). Recent weathering studies on flue gas desulfurization (FGD) wastes have shown that decreases in aqueous oxyanion concentration were concomitant with ettringite formation and that their concentration in equilibrium with ettringite are very low (*10*, *11*).

* Corresponding author present address: MS 90-1116, Earth Sciences Division, Lawrence Berkeley National Laboratory, Berkeley, CA 94720. Telephone: (510)486-4591; fax: (510)486-5105; e-mail: smyneni@lbl.gov.

† The Ohio State University.

‡ Stanford University.

Ettringite is commonly found in weathered cements, cement-based waste solidification byproducts, alkaline fly ashes, and FGD wastes. This mineral is stable at pH values >10.7, and it is one of the first phases that precipitate during the weathering of these alkaline materials (*16*, *17*). In addition to the SO_4 end member ettringite, numerous cationic and anionic substituted ettringites have been reported from natural materials and laboratory syntheses (*18*−*21*). Such extensive substitution and solid-solution formation in ettringite is possible because of its column and channel-like structure (*21*) (Figure 1).

Anion substitution in ettringite can take place either by reacting with surface sites (ligand exchange) or by substituting inside the channels for sulfate (isomorphic substitution). While As(V) substitution in ettringite has been previously observed (*19*), the extent of substitution was thought to be limited by differences in ionic charge and size (when compared to sulfate). Clearly, ettringite has a high affinity for aqueous As(V), but ettringite total sorption capacity and stability have not been determined. The present study postulates possible mechanisms of ettringite As(V) sorption and addresses this aspect by (1) evaluating ettringite As(V) sorption under different pH and ettringite suspension concentration, (2) examining sorption differences during As(V) adsorption (presumably only surface coverage) and coprecipitation [As(V) incorporation into ettringite channels and solid solution formation], and (3) assessing As(V) desorption from adsorbed and coprecipitated arsenic ettringite.

Experimental Materials and Methods

Materials. Deionized water used in these studies (Barnstead, NANOpure II system) was boiled for 1 h followed by cooling under ascarite in a N_2(g)-filled glovebox to eliminate CO_2(aq). This procedure was repeated prior to each experiment. Acid-washed Teflon and polypropylene bottles and centrifuge tubes were used in all experiments. Reagent-grade CaO (Aldrich), $Al_2(SO_4)_3\cdot 16H_20$ (Baker), sucrose (Jenneile), $NaClO_4$ (GFS), Na_2SO_4 (Baker), $Na_2(HAsO_4\cdot 7H_2O)$ (Aldrich), NaOH (Jenneile), and HCl (EM Science) were used as supplied.

Synthesis of Sulfate Ettringite. Ettringite was synthesized under N_2(g) by mixing $Al_2(SO_4)_3$ and CaO in a 10% sucrose solution. The X-ray diffraction (XRD) patterns and the chemical analysis of the precipitated solids indicated that the synthesized material was ettringite, and this material was used in all adsorption experiments. Details of the synthesis procedures and the precipitate chemical analysis and stoichiometry are given elsewhere (*16*). Scanning electron microscopy (SEM) images of synthetic ettringite prepared by this procedure exhibited crystals with a short prismatic habit, and these were significantly smaller than those made in the absence of sucrose (*20*, also see Figure 5).

Synthesis of Adsorbed and Coprecipitated Arsenic(V) Ettringite. Two coprecipitated [solid-phase As(V) ∼ 0.18, 0.30 mol kg^{-1}) and one adsorbed arsenic ettringite [solid-phase As(V) ∼ 8.3 mmol kg^{-1}] samples were synthesized to examine the extent of As(V) desorption from ettringite. Sucrose was not used in this synthesis to minimize its complexation with As(V). All these synthesis procedures were conducted at pH 11.5 (maintained by NaOH) to prevent gypsum formation (details provided in ref 16).

Methods. Aqueous concentrations of total Al, Ca, arsenate, and sulfate are referred to as Al, Ca, As(V), and sulfate, respectively, in the text. The concentration of free ions or complexes are represented with their symbols and corresponding charges.

Reactive Site Density Analysis. The number of reactive sites on ettringite external surfaces was estimated using

S0013-936X(96)00759-6 CCC: $14.00

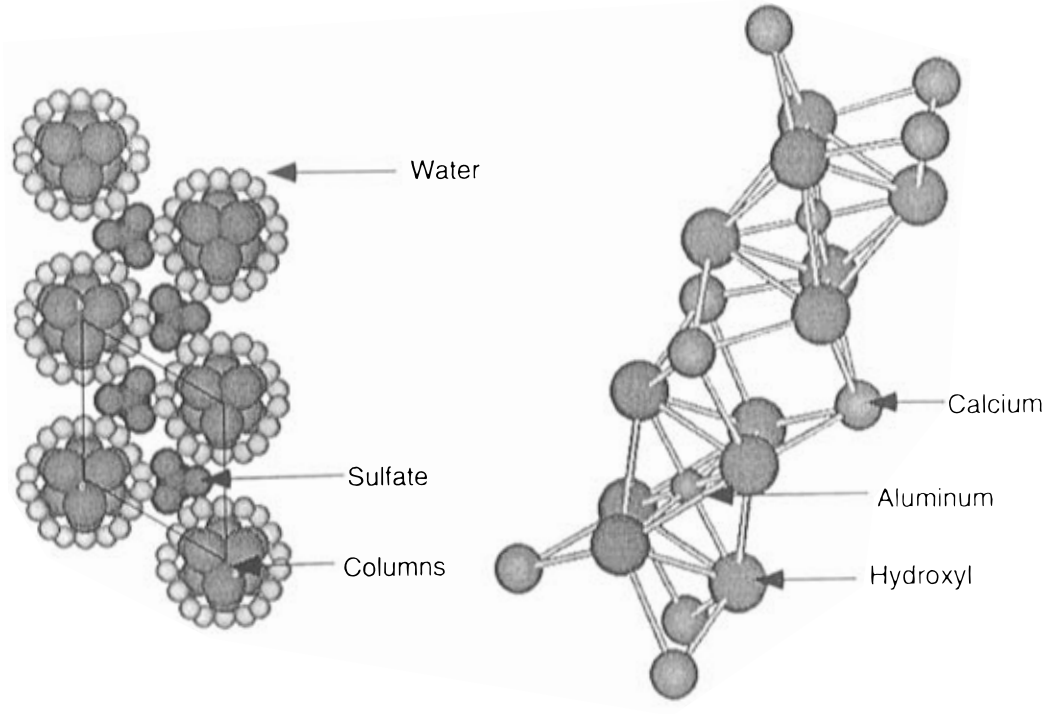

FIGURE 1. Structure of ettringite. (A) Perpendicular to *c*-axis [(001) plane], showing columns and channels. (B) Structure of a single column showing Al polyhedra and part of Ca polyhedra. Calcium-coordinated H_2O is removed for clarity. The structure is created using MOLEVIEW (a crystallographic software) and the crystal refinement data of Moore and Taylor (*21*).

ettringite surface area and its unit cell composition. Single-point surface area measurements were made with a Micromeritics Flow Sorb II 2300 BET surface area analyzer. The instrument was calibrated with specimen kaolin (standard 8570, surface area = 10.3 $m^2 g^{-1}$) and alumina (standard 8571, surface area = 153 $m^2 g^{-1}$) supplied by Micromeritics.

As(V) Adsorption Studies. Preliminary batch adsorption experiments showed that equilibrium between ettringite and As(V) was essentially instantaneous (apparent equilibrium was established before the samples could be filtered). Solution composition was invariant from <1 min to 96 h, and thus a 24-h reaction time was adopted for all adsorption experiments for convenience. Stock solutions were prepared for different As(V) concentrations by dissolving $Na_2(HAsO_4)\cdot 7H_2O$ in CO_2-free deionized water. In all adsorption experiments, these solutions were reacted with synthetic ettringite at different suspension concentrations. All samples were reacted at 298 (± 1.0) K on an oscillating shaker. After 24 h, the samples were centrifuged, the supernatant pH was recorded, and the solutions were filtered through 0.20 μm polycarbonate membranes and saved for analysis of Ca, Al, Na, As(V), and sulfate. In pH-controlled experiments, 0.1 M NaOH and HCl were used to attain required pH.

Coprecipitation Studies. Ettringite was precipitated from mixed As(V) and sulfate solutions during coprecipitation. Initially 100-mL aliquots of solutions containing dissolved $Al_2(SO_4)_3\cdot 16H_2O$ and $Na_2HAsO_4\cdot 7H_2O$ were prepared to provide a range of As(V)/sulfate ratios. To each of these solutions, 0.13 g of CaO slurry was added, and the resultant suspension was stirred for 24 h, after which the suspension was centrifuged, the supernatant pH was recorded, and the solutions were analyzed for elemental composition as described below. The suspension concentration in these samples was approximately 1.2 g L^{-1}, and the solid-phase As(V) concentration was calculated from mass balance.

Desorption Studies. The ability of sulfate to displace adsorbed and coprecipitated As(V) from arsenic ettringite was examined in CO_2-free sulfate solutions with and without ionic strength control. In the latter case, 25 mL of 2.08−20.83 mM sulfate was reacted with coprecipitated arsenic ettringite (0.1 g containing 0.30 mol kg^{-1}) for 336 h. The desorption was relatively rapid and reached equilibrium before supernatant was separated. In ionic strength-controlled experiments, 0.1 g of adsorbed [solid-phase As(V) = 8.3 mmol kg^{-1}] and coprecipitated [solid-phase As(V) = 0.18 mol kg^{-1}] arsenic ettringite were reacted with 2.08−20.83 mM sulfate in the presence of sufficient $NaClO_4$ to obtain initial ionic strengths of 0.1, 0.3, 0.5, and 1.0 $mol_c\ L^{-1}$. Since the desorption kinetics were relatively rapid, a 24-h reaction time was considered in these experiments for convenience. The samples were filtered after the reaction, and the resultant solids and solutions were analyzed as described below.

Instrumentation. The reacted solid sample mineralogy was examined with XRD and SEM. The XRD patterns were collected using a Philips 3100 X-ray generator and a Philips PW 1216/90 wide range goniometer. The diffraction scans ranged from 6 to 55° 2θ with a step interval of 0.05° 2θ and a counting time of 4 s per step. The sample d-spacings were compared with the data from the International Center for Diffraction Data (ICDD) search manual. A JEOL JSM-820 SEM was used to study reacted sample mineral morphology. An Orion expandable ion analyzer EA 920 connected to a Ross pH electrode (8103) was used to measure solution pH, and these measurements were made in particle-free supernatants. Dissolved cations were analyzed with a Perkin-Elmer 3030B atomic absorption spectrometer (AAS). A Dionex 2000i basic chromatography module (IC) (Dionex AS4A 4-mm separator column, AG4A guard column) was used for most anion concentration measurements. A Perkin Elmer 4100ZL graphite AAS and a Leeman PS2000 inductively coupled plasma (ICP) spectrometer were used to measure dilute (<0.014 mM) and concentrated As(V) samples, respectively. The samples with perchlorate matrix were analyzed by ICP for both cations and anions. Reference solutions supplied

by GFS Chemicals were used to calibrate the IC, AAS, and ICP instruments.

Results

Reactive Surface Sites and Site Density. The columns of ettringite crystals are made of $\{Ca_6[Al(OH)_6]_2 \cdot 24H_2O\}^{6+}$, and the intercolumn SO_4^{2-} holds the columns together through electrostatic interactions (Figure 1) (*21*). The column Al is in octahedral coordination with 6 OH, and Ca atoms are in 8-fold coordination with 4 OH and 4 H_2O molecules. These Ca-coordinated H_2O molecules are projected into the channels and surround the outer-sphere sulfate ions. Thus ettringite surfaces consist of $\equiv CaOH_2$, $\equiv Ca_2OH$, and $\equiv AlOH$ functional groups and, of these, the $\equiv CaOH_2$ functional groups are predominant (>90%).

Structural analysis based on the bond valence rule (*22*) suggests that the charge contribution from cations at O atoms are 0.18, 0.61, and 0.51 vu (valence units) (excluding proton influence) for $\equiv CaOH_2$, $\equiv Ca_2OH$, and $\equiv AlOH$ functional groups, respectively. The charge donation from a proton is not considered here, since O−H bond lengths of surface OH moieties are difficult to predict because of their extensive H-bond formation with solvent/adsorbed H_2O molecules. However, AsO_4^{3-} adsorption always results in surface hydroxyl displacement since the O atom in protonated AsOH is already saturated (AsO 1.25 vu, OH ∼ 0.78 vu). After AsO_4^{3-} adsorption, Ca−O bonds may shorten to similar distances as observed in calcium arsenate solids, and the remaining charge on O can be balanced through H-bonding with neighboring H_2O in the same polyhedra or solvent.

During adsorption, As(V) may interact with all three types of $\equiv CaOH_2$, $\equiv Ca_2OH$, and $\equiv AlOH$ functional groups and may form corner-sharing $\equiv CaOAsO_3$, $\equiv Ca_2OAsO_3$, and $\equiv AlOAsO_3$ complexes, respectively. After As(V) complexation, bond valence at the linking O atom of the above complexes would be 1.43, 1.85, and 1.76 vu, respectively. Thus, the O atom in $\equiv CaOAsO_3$ complex needs more vu (0.57) from other cations as compared to the other two types of complexes (0.15 and 0.24 vu) to satisfy electroneutrality. Although H-bonding with surrounding solvent H_2O can fill in this balance (0.57 vu, i.e., H-bonding with 3 H_2O molecules) on ettringite external surfaces, such interactions are limited inside the channels, since free H_2O molecules are not available. Thus, direct arsenate inner-sphere complex formation with column $\equiv CaOH_2$ and formation of $\equiv CaOAsO_3$ complexes inside the channels are restrained, and this limits As(V) interactions to only outer-sphere ion pairs. On the other hand, other surface functional groups ($\equiv Ca_2OH$, $\equiv AlOH$) can form inner-sphere $\equiv Ca_2OAsO_3$ and $\equiv AlOAsO_3$ complexes, balance the required low vu at the O atom (0.15 and 0.24 vu, respectively) by forming only one or two H-bonds with H_2O molecules, and satisfy electroneutrality.

An edge-sharing As(V) complex formation has to satisfy the same conditions discussed above for corner-sharing complexes. In addition, the dimensions of Ca, Al, and As polyhedra edges should be similar. Also, the fixed As(V) polyhedra geometry in edge-sharing complexes do not allow extensive H-bonding with H_2O molecules. This limits the formation of edge-sharing complexes with $\equiv CaOH_2$ sites. However, the surface $\equiv Ca_2OH$ sites are suitable for edge-sharing complex formation.

The reactive surface site density estimate based on all of the surface sites indicate that the sorption maximum for synthetic ettringite is 0.11 mol kg^{-1}. Although a fraction of these total sites are truly available for reaction, sorption above this critical value clearly indicates processes other than surface reactions (channel substitution and/or calcium/aluminum arsenate precipitation). In contrast, As(V) can substitute inside the channels more easily during coprecipitation, and ettringite structure should be maintained when solid-phase As(V) concentrations approach 0.11 mol kg^{-1}.

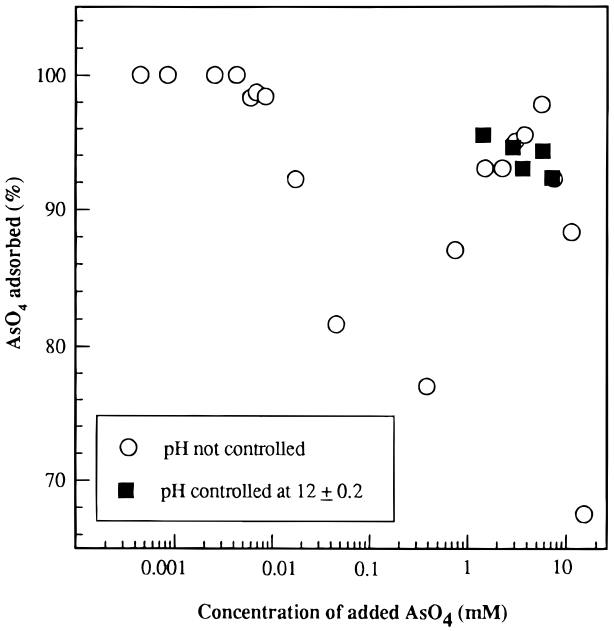

FIGURE 2. Efficiency of As(V) removal by ettringite during adsorption.

TABLE 1. Arsenate Adsorption by Ettringite at Low Initial As(V) Concentrations[a]

	[As(V)] (μM)		
		final	
sample	initial	mean	SD
1	46.0	9.01	0.5
2	17.5	1.37	0.23
3	8.57	0.14	0.01
4	6.85	0.09	0.02
5	6.00	0.10	0.01
6	4.28	BDL	
7	2.56	BDL	
8	0.85	BDL	
9	0.45	BDL	
10	0.0	BDL	

[a] Equilibrium Ca, Al, and sulfate concentrations remained constant at 2.3 ± 0.1, 0.95 ± 0.02, and 1.28 ± 0.03 mM, respectively. Abbreviations: BDL, below detection limit (0.0001 mM); SD, standard deviation.

As(V) Adsorption. Experiments were conducted for As(V) adsorption at different initial aqueous As(V) concentrations (0.45 μM−15.2 mM), pH (10.5−12.5), and suspension concentrations (4, 10, 20, and 30 g L^{-1}). Ionic strength was not maintained by electrolyte addition to minimize electrolyte ion substitution in ettringite. Despite the lack of a background electrolyte, sample ionic strength varied <10% in these experiments.

Ettringite As(V) sorption from aqueous solution was >98% when the initial dissolved As(V) concentration was <17 μM [corresponding solid-phase As(V) concentration <4.03 mmol kg^{-1}] (Figure 2). In this concentration range, As(V) sorption did not result in detectable changes in dissolved sulfate, Al, Ca, or pH (Table 1). As the aqueous As(V) concentration increased from 0.02 to 0.5 mM [corresponding solid-phase As(V) concentration of 4−90 mmol kg^{-1}, respectively], As(V) sorption decreased from >90% to 75%. In the concentration range of 1−10 mM As(V), sorption was >90%; it decreased steeply above this concentration range. In contrast to the results observed at dilute As(V) samples (<17 μM), concentrated As(V) solution interactions with ettringite resulted in changes in dissolved sulfate, Al, Ca, and solution pH. Concomitant with increases in the sorbed As(V) concentration, equilibrium pH decreased from 11.4 to 10.9. Dissolved

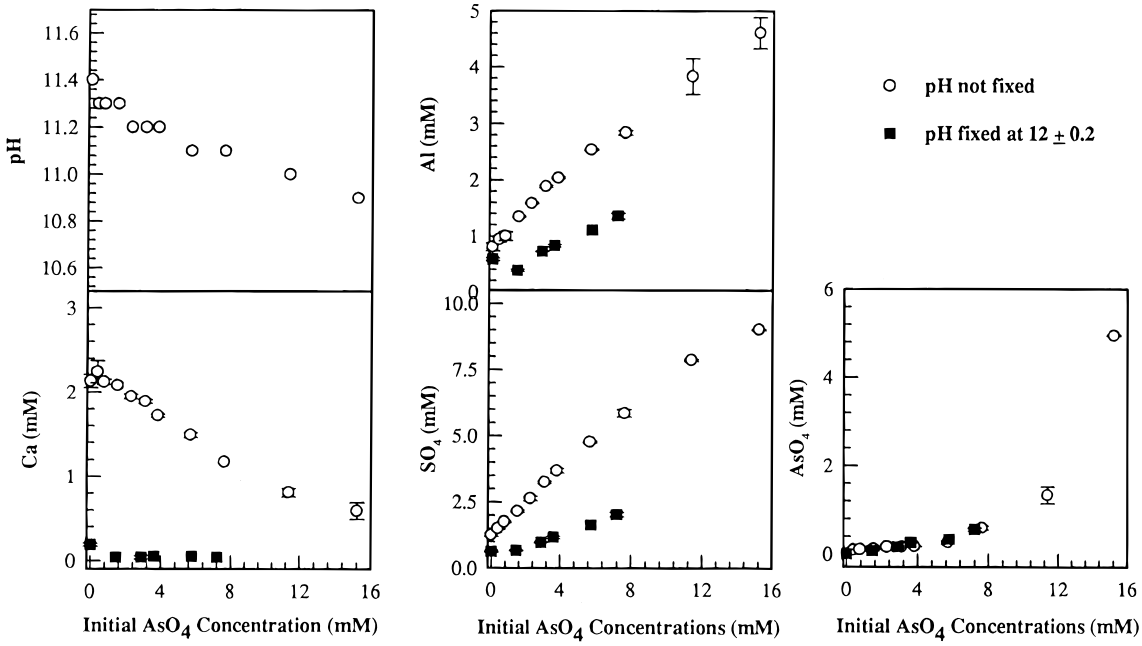

FIGURE 3. Adsorption of As(V) in ettringite.

Ca also showed a similar trend and decreased from 2.2 to 0.6 mM, and corresponding sulfate and Al increased from 1.2 to 9.0 mM and from 0.8 to 4.6 mM, respectively (Figure 3).

Chemical speciation and saturation index (SI) calculations were performed using MINTEQA2 (*23*). Since ettringite dissolution buffers solution pH around 11.5, the dominant aqueous As(V) species in this system are $HAsO_4^{2-}$ and AsO_4^{3-} (*24*). SI calculations indicate that the experimental samples were undersaturated with respect to As_2O_5 and gypsum ($CaSO_4.2H_2O$) and close to saturated or supersaturated for $Ca_3(AsO_4)_2{\cdot}6H_2O$, glauberite [$Na_2Ca(SO_4)_2$], and gibbsite [$\gamma$-$Al(OH)_3$]. The available thermodynamic data on As(V)-containing minerals is limited and equilibrium constants (K_{sp}) are listed only for $Ca_3(AsO_4)_2{\cdot}6H_2O$ and As_2O_5. Although previous studies on calcium arsenate systems suggest that $Ca_4(AsO_4)_2(OH)_2{\cdot}4H_2O$ can precipitate when As(V)-containing solutions are added to CaO slurries, its solubility product constant has not been reported (*13*). We found that concentrated aqueous As(V) (>72 mM) interactions with CaO at ambient temperature and pressure precipitated johnbaumite, $Ca_5(AsO_4)_3(OH)$, $pK_{sp} = 39.60$ (*16*).

Repeating the MINTEQA2 calculations with johnbaumite in the thermodynamic database indicated that the concentrated adsorption samples [solid-phase As(V) > 0.15 mol kg^{-1}] were close to johnbaumite saturation (SI = −0.17−+0.23). However, this phase was not detected by XRD (Figure 4A, panel b−e). In the absence of pH control, ettringite XRD peaks decreased in intensity with increases in sorbed As(V) (Figure 4A, panel a). Concomitantly, gypsum XRD peaks (7.63 and 4.28 Å) appeared and increased in intensity (Figure 4A, panels b and c). When the sorbed As(V) concentration reached 1.4 mol kg^{-1}, ettringite XRD peaks disappeared and only gypsum was evident (Figure 4A, panel c). It should be noted that gypsum presence in these samples was in contrast to the results of SI calculations. Similar observations were also made for gypsum precipitation in acidic mine waters (C. N. Alpers, personal communication). At higher As(V) loadings, gypsum also completely disappeared, and one or more new solids precipitated. These latter samples showed some sharp XRD peaks with a broad uneven baseline, indicative of poorly crystalline material, and did not correspond to any solids reported in the ICDD manual. The results were quite different when a constant pH of 12.0 (± 0.2) was maintained. Gypsum was absent in the XRD patterns, and ettringite persisted at all As(V) loadings (0.34−1.66 mol kg^{-1}) (Figure 4A, panels d and e). However, these sample XRD scans exhibit a decrease in intensity for ettringite reflections, and the presence of poorly crystalline phases in more concentrated samples (Figure 4A, panel e).

SEM indicated that synthetic ettringite was fine-grained, needle-shaped, and 2 μm in length (Figure 5a). As these samples were reacted with As(V) solutions, the ettringite presence decreased and large gypsum euhedral crystals (~20 μm) appeared. However, at higher As(V) concentration (As(V) > 0.8 mol kg^{-1}), gypsum crystals exhibited dissolution features such as etch pits and lost their clear euhedral geometry (Figure 5b). The precipitates at the highest solid-phase As(V) concentration were fine grained (<1 μm) and difficult to image with SEM.

Effect of Suspension Concentration on As(V) Adsorption. Changes in ettringite suspension density greatly affected sorption in the examined As(V) concentration range (0.007−0.072 mM). Increases in suspension density resulted in increased As(V) sorption and aqueous sulfate, Al, and Ca concentration; solution pH decreased from 11.4 to 10.5 (Figure S1 in Supporting Information). These changes in pH, sulfate, Al, and Ca were observed even in the absence of any added As(V). The solutions reacted at all suspension concentrations were also close to ettringite saturation. Except for the lowest suspension concentration (4 g L^{-1}), Ca/Al and Ca/SO_4 ratios of the reacted solutions (approximately 2.3 and 1.70, respectively) were smaller than those of the precipitate (2.97 and 2.22, respectively), indicating incongruity in ettringite dissolution at high suspension concentration. This may be attributed to the formation of some form of surface polymers or a secondary precipitate on ettringite surfaces. Similar results have been reported for feldspar and olivine dissolution (*25*, *26*).

Effect of pH on As(V) Adsorption. Sorption of As(V) was unaffected by pH in the range of 10.5−12.2 (Figure 3). At pH 10.5, less As(V) sorption occurred as compared to high pH experiments. This likely resulted from ettringite dissolution and its markedly lower stability at pH <10.7 (*16*). Solution pH did have a strong effect on aqueous Ca, Al and sulfate across the entire range examined in this study. When pH was maintained at 12.0, As(V) sorption caused only small changes in dissolved Ca, Al, and sulfate concentration (Figure 3).

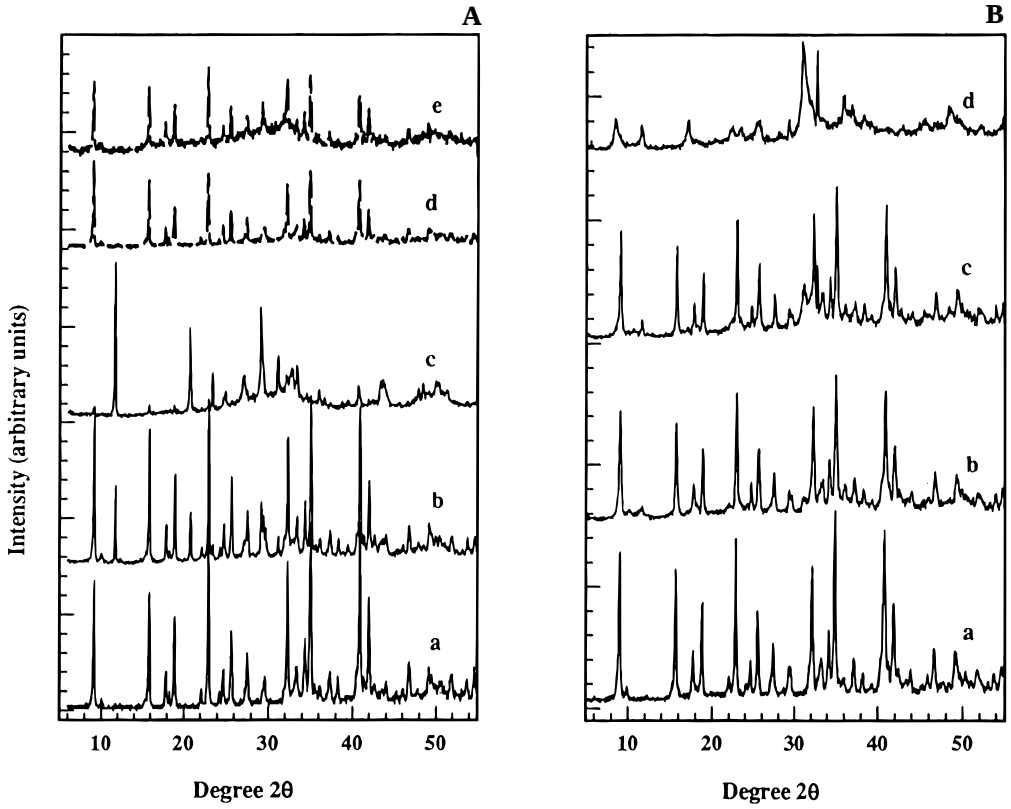

FIGURE 4. X-ray diffraction of As(V) reacted ettringites. (A) Adsorption samples: (a) pure ettringite; (b and c) reacted with 2.16 and 5.4 mM As(V) in the absence of pH control; (d and e) pH-controlled samples (pH = 12 ± 0.2) and exposed to 2.88 and 7.2 mM As(V), respectively. Suspension concentration was maintained at 4 g L^{-1}. (B) Coprecipitation samples: (a) pure ettringite; (b−d) reacted with 0.36, 1.42, and 2.52 mM As(V), respectively. Suspension concentration and pH were maintained at 1.2 g L^{-1} and 11.9 ± 0.3.

As(V) Coprecipitation. Arsenate uptake in the coprecipitation experiments (Table 2) was several fold greater than in the adsorption experiments, even at the lowest suspension concentration examined (1.2 g L^{-1}). In addition, XRD showed that ettringite was the only stable crystalline phase at all but the highest As(V) concentration (initial aqueous phase sulfate: As(V) ≈ 0:1). However, when essentially no sulfate was present during coprecipitation, a new mineral was precipitated. The structure, chemistry, and XRD of this new phase were not reported in the ICDD powder files. Even though ettringite was stable over a wide As(V) concentration range (Table 2), a flat baseline was not present in concentrated arsenic ettringite XRD (Figure 4B, panel d). Coprecipitation experiments conducted at different pHs (all above 11.0) showed that pH had no effect on either equilibrium As(V) concentration (Table 2) or on the precipitate crystal structures.

SEM showed that the adsorption and coprecipitation samples were different in their grain morphologies. The coprecipitated arsenic ettringite particles were approximately 6−10 μm in length, and with increases in solid-phase As(V) concentration, grain length decreased to approximately 2 μm (Figure 5c and d). Moreover, the grain size variation was also large at very high levels of As(V) incorporation (~2 mol kg^{-1}) (Figure 5d).

As(V) Desorption. When the rate of As(V) desorption was tested on a coprecipitated sample (0.30 mol kg^{-1}), there was no evidence of time-dependent As(V) release in the presence of sulfate, as a displacing ion (Figure S2). Although small pH changes (±0.3) were observed with time, these were within the pH measurement error. It was also found that sulfate concentration of the final filtrate was higher than the added sulfate, which was approximately 1 mM for sulfate loadings ≤5.2 mM, and higher than 2 mM when sulfate loadings were ≥10.4 mM. This sulfate increase did not correlate with increases in ionic strength or reaction time (Figure S2). However, aqueous Ca and Al concentration remained constant with time and increases in sulfate loadings.

Ionic strength-dependent desorption was measured on both adsorbed (8.3 mmol kg^{-1}) and coprecipitated (0.18 mol kg^{-1}) arsenic ettringites, at different electrolyte concentration (0.1−1.0 mol_c L^{-1} $NaClO_4$) and sulfate loadings (2.08−20.8 mM). The rationale behind selecting these two samples was that As(V) interactions in these two samples were expected to be different, i.e., dominantly surface interactions in the adsorbed sample as compared to channel substitution in the coprecipitated sample, at these solid-phase As(V) concentrations. During desorption, both sulfate and perchlorate ions can substitute inside ettringite channels and replace As(V). However, it is likely that sulfate played the dominant role in displacing As(V) because of its greater charge and smaller size. Except for As(V), adsorbed and coprecipitated sample solution chemistry was invariant for all ions during desorption.

The results of the adsorbed samples indicate that solid-phase As(V) concentration remained constant with increases in ionic strength and sulfate concentration (Figure S3a). The measured aqueous As(V) concentrations during desorption were similar to the equilibrium concentration measured during adsorption experiments (Table 1). XRD and SEM indicated no changes in sample mineralogy. On the other hand, As(V) desorption from the coprecipitated sample resulted in a release of As(V) to solution (Figure S3b). This observed As(V) release increased with increases in ionic strength and sulfate loadings and reached a plateau at high ionic strengths (>0.5 mol_c L^{-1}). The released As(V) was less than 6% of the total As(V) in the solid. When similar desorption studies were conducted on a concentrated coprecipitated arsenic ettringite [As(V) = 0.30 mol kg^{-1}], no apparent As(V) release was observed (Figure S2).

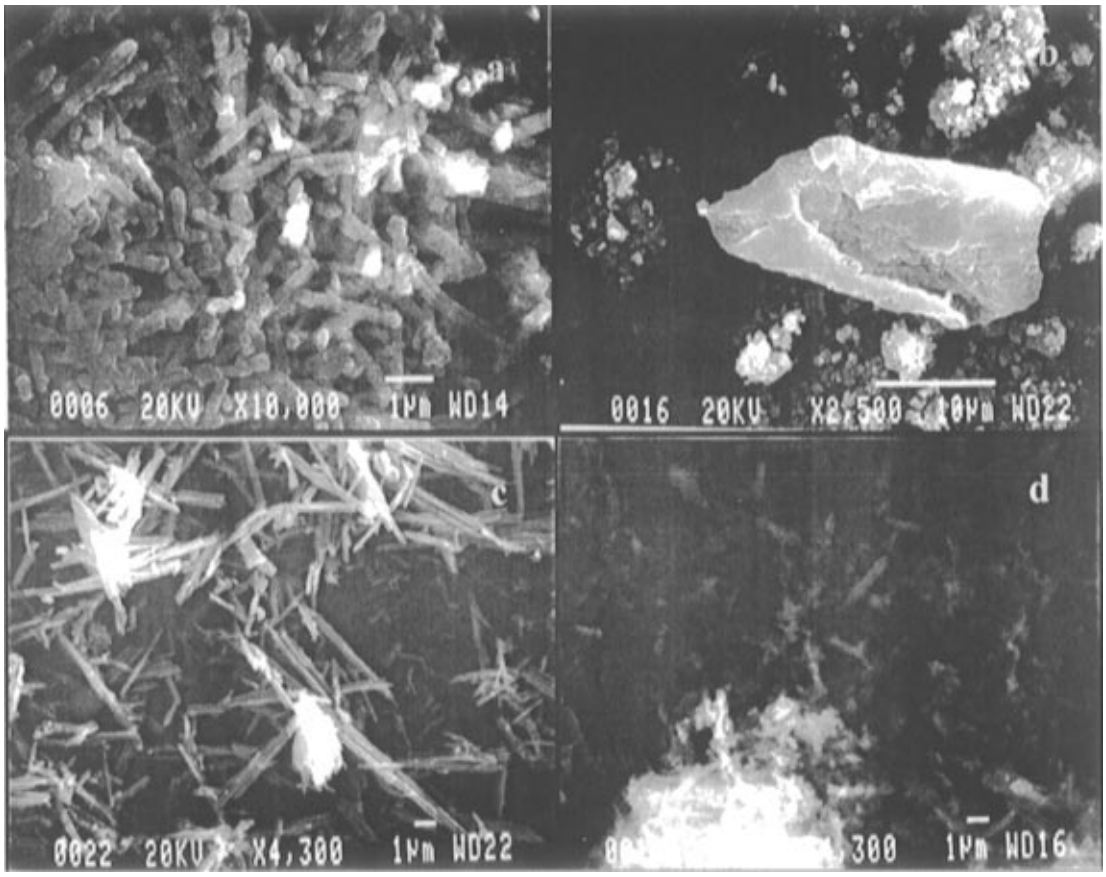

FIGURE 5. SEM micrographs of As(V) reacted ettringites: (a) Synthetic ettringite prepared using saccharate method (*16*). (b) Ettringite reacted with 5.4 mM As(V) (adsorption experiment). (c) Coprecipitated ettringite, prepared in the absence of sucrose. (d) Coprecipitated AsO_4−ettringite in the presence of 2.52 mM As(V).

TABLE 2. As(V) Coprecipitation in Ettringite[a]

As(V) initial (mM)	pH (±0.1)	As(V) equilib (mM)	$[SO_4]$ (mM) initial	$[SO_4]$ (mM) equilib
2.52	12.7	0.025	0.0	0.0
	12.8	0.013	0.0	0.0
1.44	11.2	0.009	10.4	1.21
	12.7	0.026	1.56	0.07
0.720	11.9	0.008	5.21	0.38
	12.1	0.009	5.21	0.36
	12.6	0.026	2.60	0.11
0.360	11.4	BDL	5.08	0.81
	11.5	BDL	5.21	0.68
	12.6	BDL	3.65	0.10
	12.6	0.007	2.60	0.17
0.288	12.0	BDL	4.44	0.28
	12.6	BDL	2.60	0.10
0.216	12.0	BDL	5.74	0.24
	12.6	BDL	3.65	0.09
0.144	12.5	BDL	3.60	0.05
	12.6	BDL	3.65	0.14
0.007	12.6	BDL	3.65	0.13
0.0	11.9	0.0	5.11	0.25
	12.6	0.0	3.65	0.09

[a] BDL, below detection limit (<0.005 mM). Suspension concentration, 2 g L^{-1}.

Discussion

Arsenate sorption by ettringite could result in the following: (1) surface complexation, (2) channel substitution for sulfate, and (3) precipitation of a calcium arsenate or a calcium/aluminum arsenate phase. These processes may take place simultaneously, and the information from these macroscopic experiments is insufficient to distinguish them clearly. However, the dominant mechanisms can be identified from the available solution chemistry, XRD and thermodynamic data.

Arsenate adsorption by ettringite was variable in the concentration range of 0.0005−15.5 mM As(V) (Figure 2). Adsorption at low aqueous As(V) concentration (<0.02 mM) resulted in no detectable changes in aqueous Ca, Al, and sulfate concentration. This may indicate insignificant channel substitution, which results in sulfate ion displacement from the solid and a corresponding increase in dissolved sulfate. The observed strong positive correlation between suspension concentration and As(V) uptake is characteristic of surface interactions (Figure S1). XRD suggests that the ettringite structure was preserved, and no new mineral phases were created. In addition, exposure of these arsenic ettringite samples to concentrated sulfate and high ionic strength solutions did not result in As(V) desorption (Figure S3a). These results indicate that As(V) complexes strongly with ettringite surface sites. Since ettringite surfaces are negatively charged in the experimental pH range (*27*), specific adsorption must occur through ligand exchange, i.e., by replacing Ca/Al-coordinated surface OH or Ca-coordinated H_2O.

Increases in aqueous As(V) concentration (0.02−0.2 mM) decreased its removal efficiency. The corresponding solid-phase As(V) concentrations were also close to 0.11 mol kg^{-1}, the concentration limit that indicates ettringite surface site saturation. Arsenate uptake in this concentration range resulted in sulfate release, with no detectable changes in aqueous Al and Ca concentration. In addition, a strong positive correlation between suspension concentration and As(V) uptake was also noticed (Figure S1). These results may suggest simultaneous surface interactions and channel substitution for sulfate. However, the channel sites close to the crystal edges are more accessible for substitution as

TABLE 3. AsO_4^{3-} Activity in Equilibrium with Ettringite, $Ca_3(AsO_4)_2 \cdot 6H_2O$, and Johnbaumite

sample	pH	log (Ca^{2+})	p (AsO_4^{3-}) ettringite[a]	johnbaumite	$Ca_3(AsO_4)_2 \cdot 6H_2O$
1	12.7	−2.49	<9.0[b]−5.0[c]	8.62	5.73
2	11.3	−2.86	<9.0[b]−4.0[c]	7.53	5.16
3	10.9	−3.71	3.54	5.98	3.89

[a] AsO_4^{3-} activities in equilibrium with ettringite are variable and depend on the pH, initial As(V) and sulfate, and suspension concentrations. [b] AsO_4^{3-} activity in equilibrium with ettringite when initial As(V) ~10 μM. [c] AsO_4^{3-} activity in equilibrium with ettringite when initial As(V) ~5 mM.

compared to the inner-channel sites due to slow solid-state diffusion and ion displacement. Thus, once the channel sites adjacent to the crystal edges become occupied, diffusion likely limits the access of inner-channel sites and reduces As(V) removal efficiency. This may correspond to the first observed decrease in As(V) removal efficiency at the initial As(V) concentration of 0.1 mM (Figure 2).

With further increases in aqueous As(V) concentration (>0.5 mM), As(V) uptake by ettringite increased initially before decreasing again above 10 mM As(V). In this As(V) concentration range, aqueous sulfate and Al concentration increased, and Ca concentration decreased with increased As(V) loadings. XRD and SEM indicated new unidentified mineral phases and gypsum, in addition to ettringite. These results may imply thermodynamic saturation and precipitation of a poorly crystalline phase suggested to be present from XRD. These solids may be calcium arsenate phases, since As(V) uptake resulted in Al and sulfate release into solution and corresponding retention of Ca. Precipitation of this phase may also be the reason for increased As(V) sorption in the 1−5 mM concentration range (Figure 2). Above this concentration range, all of the added ettringite was completely reacted, and this limited Ca availability for calcium arsenate precipitation. This again resulted in decreases in As(V) retention efficiency.

Although the disappearance of ettringite characteristic peaks and simultaneous development of new peaks and uneven base line in XRD of samples with As(V) concentration >1.0 mol kg^{-1} are indicative of new mineral-phase precipitation, the absence of these XRD changes in dilute arsenic ettringite samples (~0.01 mol kg^{-1}) may not completely rule out precipitation. Yet, precipitation is unlikely in these samples because (1) As(V) reactions with CaO (*16*) and γ-$Al(OH)_3$ (*16*, *28*) produced much higher equilibrium As(V) concentrations than were observed here, thus eliminating the possibility of As(V) direct interactions with calcium or aluminum oxides or the formation of calcium/aluminum arsenate precipitates; (2) precipitation of an As(V) solid phase would have resulted in uniform AsO_4^{3-} activity in reacted solutions; and (3) speciation calculations indicated low AsO_4^{3-} activities in equilibrium with ettringite as compared to the known calcium arsenates such as johnbaumite or $Ca_3(AsO_4)_2 \cdot 6H_2O$ (Table 3). In summary, surface complexation and channel substitution (channel sites close to crystal edges) at low As(V) loadings (<0.1 mM) and precipitation in concentrated samples (>0.5 mM) are the likely ettringite−As(V) sorption mechanisms.

As expected, coprecipitation resulted in larger As(V) uptake than adsorption, and this can be attributed to the greater accessibility of channel sites during coprecipitation. Although simultaneous channel and surface interactions are possible for As(V), channel substitution is preferable over surface adsorption because of the positive charge in channels (column positive charge) as compared to the surface net negative charge. In addition, As(V) sorption by ettringite well above its surface site saturation limit of 0.11 mol kg^{-1} is also indicative of extensive As(V) substitution in channels. However, SEM indicated a progressive decrease in ettringite grain size (from 6−10 to <2 μm) with increases in As(V) concentration, which may suggest that As(V) sorption severely poisoned ettringite crystal growth. Similar observations were made from theoretical calculations of organophosphonate adsorption into ettringite channels on (001) surfaces (*29*).

If As(V) substitutes inside the channels, it can be present (1) as a completely solvated ion (or OS complex, see Figure 1) and/or (2) as an IS complex by coordinating directly to column Ca. The bond valence calculations predict that the channel AsO_4^{3-} should be present as OS complexes. Ionic strength dependence oxyanion sorption and desorption can distinguish OS and IS complexes [e.g., SeO_3^{2-} and SeO_4^{2-} sorption on iron oxides (*30*)]. In this study, As(V) desorption from a dilute, coprecipitated arsenic ettringite [As(V) = 0.18 mol kg^{-1}] was found to be dependent on ionic strength and sulfate concentration. Sorbed As(V) was not completely released, and desorption reached a maximum at an ionic strength of 0.5 mol_c L^{-1}. The extent of desorption decreased with further increases in ionic strength. These experiments suggest that at least some of the As(V) is present as an OS complex inside the channels. Furthermore, the channel sites close to the mineral edges are available for desorption due to sluggish solid-state diffusion of aqueous sulfate into ettringite channels. This resulted in only partial exchange of solid-phase OS As(V). In contrast, As(V) desorption from a concentrated arsenic ettringite [As(V) = 0.30 mol kg^{-1}] resulted in no As(V) release into solution, which suggests that As(V) binds specifically to the columns (without hydration) at high As(V) concentration. Since the bond valence estimates predict that IS As(V) complexes are unlikely inside the channels, concentrated As(V) interactions in coprecipitated samples may have been due to the formation of a new calcium arsenate mineral precipitate or simultaneous channel and surface interactions.

The relatively larger size and charge of As(V) than sulfate and high affinity of surface ≡Ca_2OH and ≡AlOH sites for As(V) adsorption restrict complete As(V) substitution for sulfate inside the channels and poison ettringite crystal growth. In addition, structural sulfate, the key ion that keeps ettringite columns together, may also play a dominant role in stabilizing ettringite and accommodating As(V) in channels. The high stability of ettringite during coprecipitation and at low channel-As(V) concentration may be attributable to the relatively high sulfate concentration. In this case, As(V) is incorporated or trapped as an inclusion in ettringite during its rapid growth from aqueous solutions. Also As(V), similar to sulfate, can be present as an OS complex in channels (bond valence calculations). However, when aqueous As(V) exceeds a critical concentration, it begins to form IS complexes with surface or channel sites (by distorting Ca polyhedra) and thus poisons ettringite crystal growth. Calcium arsenate precipitation may also takes place at the same As(V) concentration. These suggested mechanisms are however tentative, and spectroscopic studies are necessary to further confirm them and to identify the critical concentration where As(V) complexation changes from OS to IS and begins to poison ettringite growth.

The results presented here demonstrate that ettringite can sorb As(V), and As(V) solubility in equilibrium with this mineral is much lower than with other known calcium arsenate minerals in alkaline pH and environmentally relevant As(V) concentrations (Table 3). The reaction mechanisms by which ettringite can retain As(V) are as follows: (1) interactions with surface functional groups on the exterior and interior of the crystals and (2) substitution into ettringite channels with displacement of sulfate through anion exchange. Predominance of one mechanism over the other likely depends on the type of sorption and solid-phase sulfate concentration. The high stability and sorption capacity of ettringite can be best utilized in the remediation of As-

contaminated alkaline wastes. Other oxyanion sorption in ettringite and spectroscopic characterization of these systems were conducted, and their results will be presented in forthcoming papers.

Acknowledgments

This research was supported by a grant from the USGS-Water Resources Program. Additional salary and research support was provided by the Ohio Coal Development Office, the Ohio State University, and the Ohio Agricultural Research and Development Center (OARDC). OARDC Journal Article No. 3297.

Supporting Information Available

Three figures and captions showing the effect of suspension concentration on equilibrium ionic concentrations and the kinetics and ionic strength dependence of As(V) desorption (4 pp) will appear following these pages in the microfilm edition of this volume of the journal. Photocopies of the Supporting Information from this paper or microfiche (105 × 148 mm, 24× reduction, negatives) may be obtained from Microforms Office, American Chemical Society, 1155 16th St. NW, Washington, DC 20036. Full bibliographic citation (journal, title of article, names of authors, inclusive pagination, volume number, and issue number) and prepayment, check or money order for $13.50 for photocopy ($15.50 foreign) or $12.00 for microfiche ($13.00 foreign), are required. Canadian residents should add 7% GST. Supporting Information is also available via the World Wide Web at URL http://www.chemcenter.org. Users should select Electronic Publications and then Environmental Science and Technology under Electronic Editions. Detailed instructions for using this service, along with a description of the file formats, are available at this site. To download the Supporting Information, enter the journal subscription number from your mailing label. For additional information on electronic access, send electronic mail to si-help@cas.org or phone (202)872-6333.

Literature Cited

(1) Parfitt, R. L. *Ad. Agric.* **1978**, *30*, 1−50.
(2) Hingston, F. J. In *Adsorption of Inorganics at Solid-liquid Interfaces*; Anderson, M. A., Rubin, A. J., Eds.; Ann Arbor Science Publishers: Ann Arbor, MI, 1981; pp 51−90.
(3) Stumm, W. *Chemistry of the Solid-Water Interface*; Wiley-Interscience Publications: New York, 1992; 428 pp.
(4) Gupta, S. K.; Chen, K. Y. *J. Water Pollut. Control Fed.* **1978**, *48*, 493−507.
(5) Merrill, D. T.; Manzione, M. A.; Peterson, J. J.; Parker, D. S.; Chow, W.; Hobbs, A. O. *J. Water Pollut. Control Fed.* **1986**, *58*, 18−26.
(6) Fuller, C. C.; Davis, J. A. In *Origin, Transport, and Fate of Arsenic-contaminated Alluvial Sediments in the Cheyenne River System, South Dakota: U.S. Geological Survey Toxic Substances in Surface Waters and Sediments Program*; Kimball, G. E., Ed.; U.S. Geological Survey Water-Supply Paper 2385; USGS: Reston, VA, 1994; Chapter E, pp 1−55.
(7) Bigham, J. M.; Carlson, L.; Murad, E. *Miner. Mag.* **1994**, *58*, 641−648.
(8) Lumsdon, D. G.; Fraser, A. R.; Russel, J. D.; Livesey, N. T. *J. Soil Sci.* **1984**, *35*, 381−386.
(9) Goldberg, S.; Glaubig, R. A. *Soil Sci. Soc. Am. J.* **1988**, *52*, 1297−1300.
(10) Fowler, R. K.; Traina, S. J.; Bigham, J. M.; Soto, U. I. *Agric. Abstr.* **1993**, 30.
(11) Hassett, D. J.; Hassett, D. F. P.; McCarthy, G. J. *Coal Ash Symp.* **1991**, *31*, 1−17.
(12) Reddy, K. J.; Gloss, S. P.; Wang, L. *Water Res.* **1994**, *28*, 1377−1382.
(13) Reardon, E. J.; Warren, C. J.; Hobbs, M. Y. *Environ. Sci. Technol.* **1993**, *27*, 310−315.
(14) van der Hoek, E. E.; Bonouvrie, P. A.; Comans, R. N. J. *Appl. Geochem.* **1994**, *9*, 403−412.
(15) Mattigod, S. V.; Rai, D.; Eary, L. E.; Ainsworth, C. C. *J. Environ. Qual.* **1990**, *19*, 187−201.
(16) Myneni, S. C. B. Ph.D. Dissertation, The Ohio State University, Columbus, Ohio, 1995, 250 pp.
(17) Solem, J. K.; McCarthy, G. J. Advanced Cementitios Systems: Mechanisms and Properties. *Mater. Res. Soc. Symp. Proc. Ser.* **1992**, *No. 245*, 71−79.
(18) Pöllmann, H.; Kuzel, H.-J.; Wenda, R. *Cem. Concr. Res.* **1990**, *20*, 941−947.
(19) Kumarathasan, P.; McCarthy, G. J.; Hassett, D. J.; Hassett D. F. P. Fly Ash and Coal Conversion By-Products: Characterization, Utilization and Disposal VI. *Mater. Res. Soc. Symp. Proc. Ser.* **1990**, *No. 178*, 83−103.
(20) Pöllmann, H.; Kuzel, H.-J.; Wenda, R. *Cem. Concr. Res.* **1993**, *23*, 422−430.
(21) Moore, A. E.; Taylor, H. F. W. *Nature* **1968**, *218*, 1085.
(22) Brown, I. D.; Altermatt, D. *Acta Crystallogr.* **1985**, *B41*, 244−247
(23) Allison, J. D.; Brown, D. S.; Novo-Gradac, K. J. *MINTEQA2/PRODEFA2, A Geochemical Assessment Model for Environmental Systems: Version 3.0*; Office of Research Development, U.S. EPA,: Athens, GA, 1990.
(24) Dove, P. M.; Rimstidt, J. D. *Am. Mineral.* **1985**, *70*, 838−844.
(25) Casey, W. H.; Banfield, J. F.; Westrich, H. R.; McLaughlin, L. *Chem. Geol.* **1993**, *105*, 1−15.
(26) Wollast, R.; Chou, L. *Geochim. Cosmochim. Acta* **1992**, *56*, 3113−3122.
(27) Chen, S.; Mehta, P. K. *Cem. Concr. Res.* **1982**, *12*, 257−259.
(28) Anderson, M. A.; Ferguson, J. F.; Gavis, J. *J. Colloid Interface Sci.* **1976**, *54*, 391−399.
(29) Coveney, P. V.; Humphries, W. *J. Chem. Soc. Faraday Trans.* **1996**, *92*, 831−841.
(30) Hayes, K. F.; Roe, A. L.; Brown, G. E., Jr.; Hodgson, K. O.; Leckie, J. O.; Parks, G. A. *Science* **1987**, *238*, 783−786.

Received for review September 9, 1996. Revised manuscript received January 27, 1997. Accepted February 5, 1997.[⊗]

ES9607594

[⊗] Abstract published in *Advance ACS Abstracts*, April 1, 1997.